New Journal of Physics
The open access journal at the forefront of physics
Deutsche Physikalische Gesellschaft DPG | IOP Institute of Physics

Gilbert damping tensor within the breathing Fermi surface model: anisotropy and non-locality

D Thonig[1,2,3] **and J Henk**[2]

[1] Max-Planck-Institut für Mikrostrukturphysik, Weinberg 2, D-06120 Halle (Saale), Germany
[2] Institut für Physik, Martin-Luther-Universität Halle-Wittenberg, D-06120 Halle (Saale), Germany
E-mail: dboettch@mpi-halle.de

Received 19 July 2013, revised 8 November 2013
Accepted for publication 12 December 2013
Published 17 January 2014
New Journal of Physics **16** (2014) 013032
doi:10.1088/1367-2630/16/1/013032

Abstract

In magnetization dynamics, the Gilbert damping α is often taken as a parameter. We report on a theoretical investigation of α, taking into account crystal symmetries, spin–orbit coupling and thermal reservoirs. The tensor $\boldsymbol{\alpha}$ is calculated within the Kamberský breathing Fermi-surface model. The computations are performed within a tight-binding electronic structure approach for the bulk and semi-infinite systems. Slater–Koster parameters are obtained by fitting the electronic structure to first-principles results obtained within the multiple-scattering theory. We address the damping tensor for the bulk and surfaces of the transition metals Fe and Co. The role of various contributions are investigated: intra- and interband transitions, electron and magnetic temperature as well as surface orientation. Our results reveal a complicated non-local, anisotropic damping that depends on all three thermal reservoirs.

1. Introduction

Magnetic devices and magnetic reversal effects are strongly affected by their rate of energy transfer (dissipation): the larger this transfer, the faster the magnetic equilibration. Regarding spintronics applications, there is an ongoing search for materials with preferably small damping [1]. The magnetization dynamics on a nanometer length scale and on a femtosecond

[3] Author to whom any correspondence should be addressed.

TH-2014-02

time scale can be described by the Landau–Lifshitz–Gilbert (LLG) equation [2]. Here, the dissipation is introduced by Gilbert's phenomenological parameter α [3] that includes all possible damping mechanisms. The damping parameter is taken as local and isotropic, in agreement with ferromagnetic resonance spectroscopy [4, 5].

The coupling of the magnetization to the electronic degrees of freedom is mediated by spin–orbit coupling. Detailed measurements on the atomic scale as well as theoretical models for nanostructures reveal a non-uniform spin–orbit coupling [6] which is responsible for local magnetic anisotropies. Hence, the Gilbert damping should also be anisotropic and site-dependent, in particular in low-dimensional systems.

To calculate the damping constant from first principles, Ebert *et al* [7] suggest a model that shows a good agreement with experiments. Based on the linear response theory, their torque–torque correlation model was applied to an $Fe_{1-x}Co_x$ alloy and to various 5d transition metals. Thermal effects are included by phonon scattering in an alloy-analogy model.

Besides linear response theory, there exists also the breathing Fermi surface model of Kamberský [8, 9]. This model considers the non-equilibrium population of electronic states that is forced by the change of the magnetic moments. The coupling of the electronic spin to the electronic eigenstates is of spin–orbit nature. The model predicts a significant damping in metals with strong spin–orbit coupling, e.g. 4f metals. Also ultrathin films are predicted to exhibit strong damping [10].

The energy change near the Fermi surface of the Stoner magnets Fe and Co has been investigated by Gilmore *et al* [11], using the Kamberský model in a projector augmented wave method. Although in good agreement with experimental findings, their results do not comply with those by Fähnle and Steiauf [12] where a dependence of the damping α on the magnetic moment's direction [13] as well as on temperature is established. The latter has been observed experimentally [14–16] and confirmed theoretically [7, 10]. The Gilbert damping for (oxidic) nanoparticles [17], Ni–Fe and Ni–Co alloys [18], half metals [1], Co/Ni multilayers [19] and magnetic thin films [20–22] were also studied recently. Such materials are recommended for spintronic applications due to their high spin–orbit coupling and, thus, enhanced Gilbert damping. Furthermore, the damping can become anisotropic and non-local [23–25], leading to a damping tensor $\boldsymbol{\alpha}_{ij}$. The anisotropic and non-local character of the magnetic damping is also achievable within the Kamberský model.

In this paper we report on a theoretical investigation of the anisotropic and non-local Gilbert damping in the framework of the Kamberský model. To calculate the damping tensor, we use a tight-binding (TB) model. The TB parameters have been obtained by fitting the electronic structures to those of a first-principles fully relativistic multiple scattering Korringa–Kohn–Rostoker (KKR) method using a genetic algorithm. Semi-infinite systems are treated by a renormalization scheme for the Green function. These together with the generalized Kamberský equation allow calculation of the layer- as well as the temperature-resolved damping tensor. We compare our results to published data for Fe and Co. The role of various contributions are analyzed in detail: electronic intra- and interband transitions, electron and magnetic temperature as well as surface orientation. Our results reveal a complicated non-local, anisotropic damping that depends on all three thermal reservoirs.

The paper is organized as follows. Computational details and theoretical basics are given in section 2. The damping properties of bulk magnets are discussed in section 3.1, for surfaces in section 3.2.

2. Theoretical and computational aspects

We consider a ferromagnetic system whose Bloch states, characterized by the band index n at wavevector $\boldsymbol{k}$, have energies $\varepsilon_{\boldsymbol{k},n}$. Due to the spin–orbit coupling, the magnetization $\boldsymbol{m}$ with direction $\boldsymbol{e}$ affects the eigenstates: tilting $\boldsymbol{m}$ by a small change $\delta\boldsymbol{e}$ generates a non-equilibrium population state which can be viewed as a deviation—or breathing—of the Fermi surface. The non-equilibrium distribution relaxes toward the equilibrium distribution within a time $\tau_{\boldsymbol{k},n}$ (relaxation time approximation). This relaxation is driven by the coupling Λ of the electron reservoir to the lattice reservoir, that is via the electron–phonon coupling. Following Gilmore *et al* [11], this breathing Fermi surface model of Kamberský [8, 9] in a generalized form and within the isotropic relaxation time approximation ($\tau_{\boldsymbol{k},n} \to \tau$) results in the damping tensor $\boldsymbol{\alpha}$ with elements

$$\alpha^{\nu\mu} = \frac{g\pi}{m} \sum_{n,m} \int \eta(\varepsilon_{\boldsymbol{k},n}) \left(\frac{\partial \varepsilon_{\boldsymbol{k},n}}{\partial \delta \boldsymbol{e}}\right)_{\nu} \left(\frac{\partial \varepsilon_{\boldsymbol{k},m}}{\partial \delta \boldsymbol{e}}\right)_{\mu} \frac{\tau}{\hbar} \frac{\mathrm{d}\boldsymbol{k}}{(2\pi)^3} \quad \nu, \mu = x, y, z, \tag{1}$$

$\eta(\varepsilon_{\boldsymbol{k},n}) = {}^{\partial f(\varepsilon)}/_{\partial \varepsilon}\big|_{\varepsilon_{\boldsymbol{k},n}}$ is the derivative of the Fermi–Dirac distribution $f(\varepsilon)$ with respect to the energy; n and m are band indices.

The spin–orbit coupling $\hat{H}_{\mathrm{so}}$ correlates the magnetization with the electronic ground state, giving rise to the magnetocrystalline anisotropy. Hence, the torque matrix elements $(\frac{\partial \varepsilon_{\boldsymbol{k},n}}{\partial \delta \boldsymbol{e}})_{\nu}$ can be obtained from $\varepsilon(\delta\boldsymbol{e}) = \langle n, \boldsymbol{k}| \mathrm{e}^{\mathrm{i}\boldsymbol{\sigma}\cdot\delta\boldsymbol{e}} \hat{H}_{\mathrm{so}}(\boldsymbol{e}) \mathrm{e}^{-\mathrm{i}\boldsymbol{\sigma}\cdot\delta\boldsymbol{e}} |m, \boldsymbol{k}\rangle$, where $|n, \boldsymbol{k}\rangle$ are the eigenstates of the Hamiltonian $\hat{H}$ and $\boldsymbol{\sigma}$ is the vector of Pauli matrices. With $\boldsymbol{\Gamma}_{nm} \equiv \langle n, \boldsymbol{k}|[\boldsymbol{\sigma}, \hat{H}_{\mathrm{so}}]|m, \boldsymbol{k}\rangle$, which accounts for the transitions between the states in bands n and m, the damping tensor $\alpha^{\nu\mu}$ reads

$$\alpha^{\nu\mu} = \frac{g\pi}{m} \sum_{n,m} \int \Gamma^{\nu}_{nm} \Gamma^{\mu}_{nm} W_{nm}(\boldsymbol{k}) \frac{\mathrm{d}\boldsymbol{k}}{(2\pi)^3}. \tag{2}$$

The scattering events depend on the overlap $W_{nm}(\boldsymbol{k}) \equiv \int \mathrm{d}\varepsilon\, \eta(\varepsilon) A^{\boldsymbol{k},n}_{\Lambda}(\varepsilon) A^{\boldsymbol{k},m}_{\Lambda}(\varepsilon)$ of the spectral function $A^{\boldsymbol{k},n}_{\Lambda}$, which is a Lorentzian centered at $\varepsilon_{\boldsymbol{k},n}$. Its width is determined by the coupling strength Λ to the lattice. Replacing the Bloch states by the Green function, the spectral function can be written as $\mathrm{Im}\,\hat{G}\,(\boldsymbol{k}, \varepsilon \pm \mathrm{i}\Lambda) = \mp \sum_n |n\rangle\langle n| A_{\Lambda}(\varepsilon - \varepsilon_{\boldsymbol{k},n})$. Hence, we end up with a result similar to the torque–torque-correlation model [7],

$$\alpha^{\nu\mu} = \frac{g}{m\pi} \int \int \eta(\varepsilon)\, \mathrm{Tr}\left(\hat{T}^{\nu}\, \mathrm{Im}\,\hat{G}\, \hat{T}^{\mu}\, \mathrm{Im}\,\hat{G}\right) \frac{\mathrm{d}\boldsymbol{k}}{(2\pi)^3} \mathrm{d}\varepsilon, \tag{3}$$

where $\hat{\boldsymbol{T}} \equiv [\boldsymbol{\sigma}, \hat{H}_{\mathrm{so}}]$.

To obtain the Green function, we use a TB model [26] based on the Slater–Koster parameterization [27, 28]. The TB parameters, including the spin–orbit coupling strength, are obtained by fitting the TB band structures to *ab initio* band structures, using a genetic algorithm [29] (table 1). The fitness function is taken from [30], with an accuracy better than 10^{-4} eV. The parameters are in good agreement with those reported in [31–33]. The first-principles band structures were calculated within a fully relativistic multiple-scattering Green function approach (KKR method) [34].

Having a reliable TB description of the bulk electronic structure at hand, we proceed by computing the electronic structure of a semi-infinite system, using a renormalization

Table 1. TB parameters for bulk bcc Fe and fcc Co, obtained from a genetic algorithm. The notation follows that of Slater and Koster [27] for the on-site energies ε (left) and hopping parameters (right). λ and B stand for orbital dependent spin–orbit coupling strength and exchange splitting, respectively. All values in eV.

	Fe	Co
ε_{s}	6.006	5.322
ε_{p}	12.658	14.000
$\varepsilon_{t_{2\mathrm{g}}}$	−0.853	−1.389
$\varepsilon_{e_{\mathrm{g}}}$	−0.955	−1.402
λ_{p}	0.200	0.100
λ_{d}	0.080	0.070
B_{s}	0.436	−0.329
B_{p}	0.793	−1.237
$B_{t_{2\mathrm{g}}}$	2.069	1.572
$B_{e_{\mathrm{g}}}$	2.034	1.526

	Fe	Co
(ssσ)	−1.494	−1.144
(spσ)	−2.035	−1.708
(sdσ)	0.769	0.435
(ppσ)	2.901	3.113
(ppπ)	−0.112	−0.204
(pdσ)	−0.903	−0.233
(pdπ)	0.303	0.510
(ddσ)	−0.623	−0.515
(ddπ)	0.412	0.387
(ddδ)	−0.066	0.093

scheme [35, 36]. The result is the layer- and site-resolved Green function, with site i in layer n indexed as $I \equiv (n, i)$. This allows the layer- and site-resolved damping tensor to be defined by

$$\alpha_{IJ}^{\nu\mu} = \frac{g}{m\pi} \int \eta(\varepsilon)\, \mathrm{Tr}\left(\hat{T}_n^{\nu}\, \mathrm{Im}\, \hat{G}_{IJ}\, \hat{T}_m^{\mu}\, \mathrm{Im}\, \hat{G}_{JI}\right) \mathrm{d}\varepsilon, \quad I \neq J. \tag{4}$$

We perform a fifth-order Keast quadrature method in the first Brillouin zone $\boldsymbol{k}$ integration with up to 10^5 mesh points for bulk and 10^6 mesh points for surface calculations. For small Λ (less than about 5×10^{-3} eV), these dense meshes are necessary to suppress spurious non-zero off-diagonal elements of the damping tensor which in principle should vanish to the cubic symmetry in bulk systems. The energy integration is approximated by a Gauss–Legendre quadrature with 32 supporting points in a small energy range around the Fermi level.

Various components of the entire system contribute to α due to different relaxation processes. This is qualitatively described by three separate but coupled reservoirs: the magnetic moments, the lattice and the electrons [37, 38], assuming the adiabatic limit. The electron temperature T_{e} is modeled by the width of the Fermi distribution, whereas the temperature of the magnetic system, the spin temperature T_{s}, is mimicked within the disordered local moment (DLM) theory which is based on the coherent potential approximation (CPA) [39, 40]. For the time being, the electron–phonon coupling is set constant. The above tensorial representation yields furthermore the dependence of the Gilbert damping on the magnetization direction, $\boldsymbol{\alpha}_{IJ} = \boldsymbol{\alpha}_{IJ}(\boldsymbol{e})$, which is mediated by the spin–orbit coupling.

The calculated Gilbert damping is used in an atomistic formulation of the LLG equation [2, 3, 41]. The temporal evolution of the magnetic moment $\boldsymbol{m}_i$ at site i reads [23, 24]

$$\frac{\partial \boldsymbol{m}_i}{\partial t} = \boldsymbol{m}_i \times \left(-\gamma \mathbf{B}_i + \sum_j \frac{1}{|\boldsymbol{m}_j|} \alpha_{i,j} \frac{\partial \boldsymbol{m}_j}{\partial t}\right). \tag{5}$$

The effective field $\mathbf{B}_i = {}^{\partial \hat{H}_{\mathrm{mag}}}/_{\partial \boldsymbol{m}_i}$ is fixed by the Hamiltonian $\hat{H}_{\mathrm{mag}}$ which comprises the Heisenberg exchange interaction, the dipole–dipole energy, the magnetocrystalline anisotropy and a Zeemann term. Explicitly,

$$\hat{H}_{\mathrm{mag}} = -\sum_{ij} \boldsymbol{m}_i \mathbf{l}_{ij} \boldsymbol{m}_j + \sum_i \mathbf{B}_{\mathrm{ext}} \cdot \boldsymbol{m}_i. \tag{6}$$

$\mathbf{I}_{ij} = J_{ij}\mathbf{E} + \mathbf{Q}_{ij}$ for $i \neq j$ contains the Heisenberg exchange parameter J_{ij} and the dipolar interaction matrix $Q_{ij}^{\nu\mu} = \frac{1}{2}\frac{\mu_0}{4\pi}\frac{3r_{ij}^{\nu}r_{ij}^{\mu} - r_{ij}^2\delta^{\nu\mu}}{r_{ij}^5}$ between two sites i and j with distance $\boldsymbol{r}_{ij} = \boldsymbol{r}_i - \boldsymbol{r}_j$. $\mathbf{E}$ is the unit matrix. $\mathbf{I}_{ii}$ determines the magnetocrystalline anisotropy. The Heisenberg exchange interactions J_{ij} as well as the anisotropies $\mathbf{I}_{ii}$ have been calculated from first principles within the KKR framework, using the Lichtenstein formula [42] and the magnetic force theorem [34]; for details see [43].

3. Results and discussion

3.1. Damping constant of bulk materials

In this section, we first address the two approaches to α, (1) and (3), and compare our TB data to the *ab initio* results reported in [11]. We assume a ferromagnetically ordered system with magnetic moments in $\boldsymbol{e}_z$ direction. Tilting a magnetic moment toward $\boldsymbol{e}_x$ or $\boldsymbol{e}_y$ yields an effective torque matrix element $T^- \equiv \langle n, \boldsymbol{k}|[\sigma^-, \hat{H}_{\mathrm{so}}]|m, \boldsymbol{k}\rangle$, where $\sigma^- \equiv \sigma^x - \mathrm{i}\,\sigma^y$. The cubic symmetry in bulk bcc Fe and fcc Co dictates that the damping tensor is diagonal, in agreement with our calculations. The damping constant α is then given by the trace of the damping tensor $\boldsymbol{\alpha}$ for the reference magnetization direction $\boldsymbol{e}_z$ ($\alpha = \alpha^{xx} + \alpha^{yy}$) [11].

The reliability of our TB parameterization is proven by the agreement of the damping constant α with those reported in [11] (figure 1). For comparison, the TB damping constants have to be scaled by a factor of $1/4\pi^2$, which we attribute to a different definition of the Lorentzian in [11].

For large electron–phonon coupling Λ, α decreases, which is interpreted as follows. α comprises both intraband transitions ($n = m$ in (2); blue line in figure 1) and interband transitions ($n \neq m$; green line in figure 1) [11]. Energy levels n and m located close to each other accelerate the relaxation of the electron–hole pairs and, thus, decrease the Gilbert damping. The phonon reservoir 'smears out' the electron bands: the broadening of the electron spectral density is larger, the stronger electrons and phonons are coupled. Thus, the probability of transitions between states n and m is increased. For small Λ, the intraband transitions play a major role, where $\alpha^{\mathrm{intra}}(\Lambda)$ can be approximated linearly. For large Λ, the broad Lorentzians overlap (cf figure 3(a)) and lead to an increase of the interband contribution which eventually dominates the intraband contribution. This allows hopping of the electrons between states n and m. For even larger Λ, the Gilbert damping drops again, resulting in the maximum at $\Lambda \approx 1$. However, this is an artifact of the finite orbital basis in the TB approach which does not describe well electronic states far off the Fermi level (at $\approx 10\,\mathrm{eV}$). Nevertheless, the approach reproduces the *ab initio* results of [11] in the range $\Lambda \in [0.001, 1]$ well.

In the 'Lorentz' approach (2), the coupling Λ defines the width of the energy window in which transitions Γ_{nm} are accounted for; the electronic structure itself is unaffected. In the Green function approach, Λ is taken as the imaginary part of the energy at which the Green functions is evaluated. This offset from the real energy axis provides a more accurate description with respect to the *ab initio* results [11] than the Lorentzian approach, in particular for Fe. This may be understood from the fact that a finite Λ broadens and shifts maxima in the spectral function; hence, electronic states at energies around the Fermi level that are weakly weighted by $\eta(\varepsilon)$ contribute to the damping. Furthermore, their contribution depends on their orbital composition and on the strength of the spin–orbit coupling.

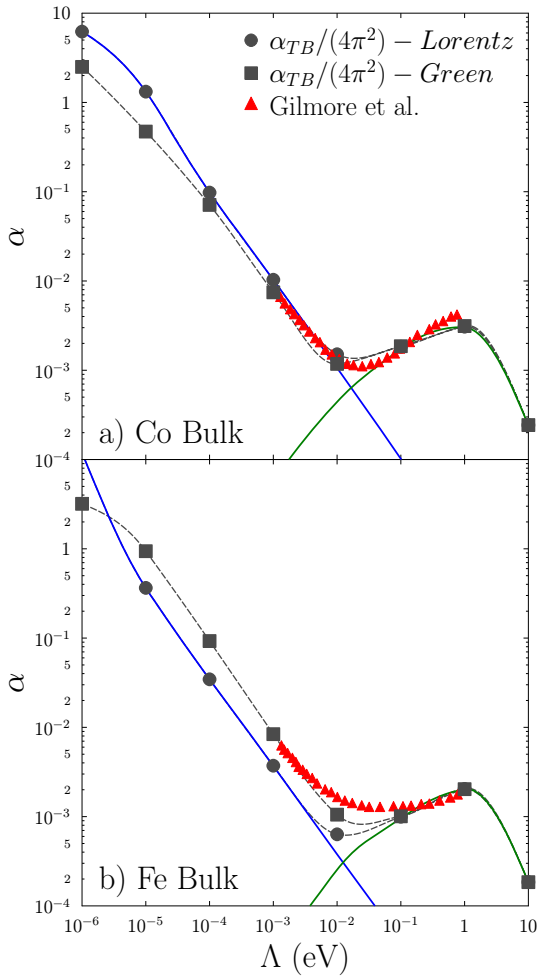

Figure 1. Calculated bulk Gilbert damping constant α versus phonon coupling strength Λ for Co (a, top) and Fe (b, bottom), in logarithmic scale. The results obtained by our TB method base on Lorentz broadening (black circles) or on Green functions (black squares). The curvature close to the minima is a superposition of inter- (green line) and intraband (blue line) transitions; the latter vanish for large Λ. Data reproduced from [11] ('Gilmore *et al*') are presented as red triangles. The dotted lines are guides to the eye.

We now discuss the dependence of α on the reservoir temperatures and focus first on the spin temperature T_s. The dependence of α on the magnetic moment direction $\boldsymbol{e}$, on the electron–phonon coupling Λ as well as on transitions involving energetically lower states suggests a correlation between the spin, lattice and electron temperature [44]. The spin temperature T_s is modeled within the DLM theory [45, 46]. This approach is based on a substitutional binary alloy that is described within the CPA [39, 40, 47]; the host material comprises sites with magnetization along the reference direction $\boldsymbol{e}$, with concentration $c_{\Uparrow}$, and sites with magnetization along $-\boldsymbol{e}$, with concentration $c_{\Downarrow} = 1 - c_{\Uparrow}$ [48] (figure 2). Zero spin temperature is obtained for $c_{\Uparrow} = 1.0$ (ferromagnetic case), whereas the critical temperature is given for $c_{\Uparrow} = 0.5$ (paramagnetic case). The mapping of the impurity concentration on the spin temperature can be obtained by comparing magnetizations derived from DLM electronic-structure calculations and from temperature-dependent Monte Carlo calculations [48, 49].

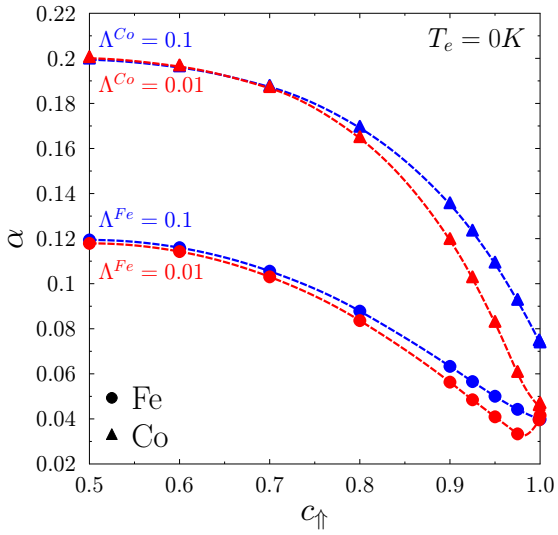

Figure 2. Damping constant α versus spin temperature T_s for bulk Co (triangles) and Fe (circles), as modeled by the concentration $c_{\Uparrow}$ in the DLM theory (see the text). The concentration is inversely proportional to the temperature [48]. Data for electron–phonon coupling $\Lambda = 0.1$ eV(0.01 eV) are displayed in blue (red). The electron temperature T_e is zero. Lines serve as guides to the eye.

The dependence of α on the spin temperature (figure 2) is in agreement with the dissipation-fluctuation theorem which states, roughly speaking, that the dissipative reaction of the system is proportional to the fluctuation. Here, the electron system tries to stabilize the magnetic order with increasing T_s (that is increasing magnetic fluctuations or decreasing concentration) by increasing the Gilbert damping which models the dissipation. The sizable change of α with concentration suggests that a constant α may be inappropriate for modeling magnetic systems at elevated temperatures, for example using the LLG equation.

We now turn to the dependence of α on the electron temperature T_e. The electron temperature is included via η in (1) and accounts for transitions between states in a narrow energy window above the Fermi level. An electron–hole pair relaxes faster from the non-equilibrium population (which is induced by the spin–orbit coupling) toward the equilibrium than in the zero temperature case; thus, α decreases with decreasing relaxation time τ. This mechanism is contrasted by the fact that more electronic states around the Fermi level are involved in the relaxation process, leading to an increase of α. Hence, the Kamberský model postulates a competition between these two mechanisms (figure 3).

We limit the dependence of α on the electron temperature by the energy window around the Fermi level ε_F to $\varepsilon_{cut} = 0.01, 0.1$ and 1.0 eV (figure 3). For a large energy window of $\varepsilon_{cut} = 1$ eV, α (T_e) increases nonlinearly with electron temperature; a similar trend is found for the magnetic temperature T_s. This finding is explained by the large spectral overlap W_{nm} (figure 3(a)): W_{nm} is constrained by the derivative η of the Fermi–Dirac distribution. The higher the temperature, the larger the spectral overlap (color shaded areas in figure 3(a)) and therefore, α increases. If ε_{cut} is smaller than the underlying range of the Fermi–Dirac distribution, α decreases with the temperature.

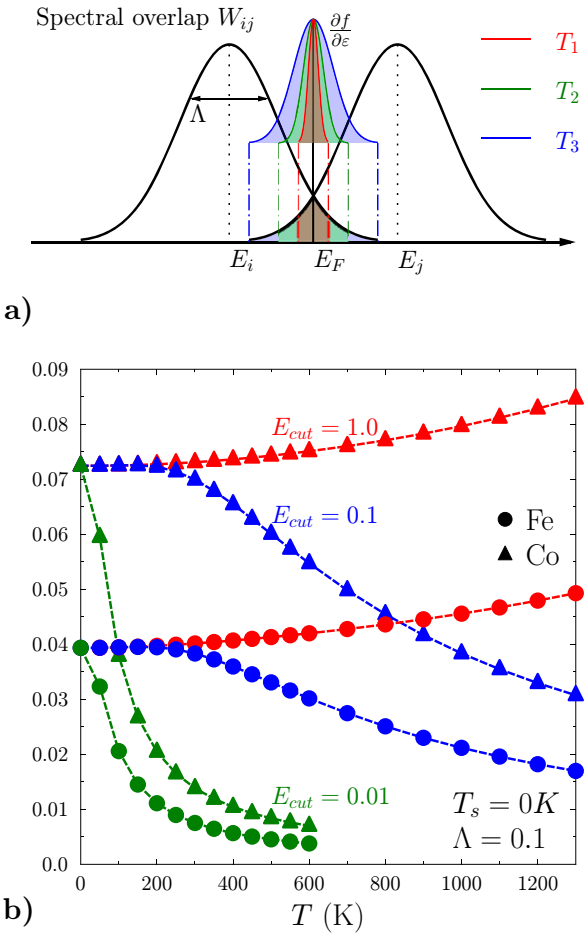

Figure 3. (a) Illustration of the spectral overlap contribution between electronic state i and j for temperatures $T_1 < T_2 < T_3$. With increasing temperature the relevant energy window around the Fermi energy E_F becomes larger, leading to an increased Gilbert damping α. (b) α versus electron temperature T_e for a fixed electron–phonon coupling $\Lambda = 0.1$ for Co (triangles) and Fe (circles). Energy cut-offs are distinguished by colors: $\varepsilon_{cut} = 0.01$ eV green, 0.1 eV blue and 1.0 eV red. The spin temperature T_s is zero. Lines serve as guides to the eye.

The electron–phonon coupling is, at present, roughly modeled by a constant Λ. Phonons can be included via the spatial dependence of the TB parameters, for example using Harrison's law [28] or by a polynomial representation [50]. In particular the latter reproduces well phonon dispersions. The atomic displacements change the electronic structure around the Fermi level and remove degeneracies in the band structure; thus, the accompanying decrease of contributions from intraband transitions will reduce α [7]. In addition, electron–magnon scattering or the Eliott–Yafet-type spin scattering mechanism could be included [51].

The damping tensor (1) motivated in [12, 13] accounts for transitions between states with different reference spin direction and, thus, also for spin–flip transitions. For cubic symmetry, the damping tensor is diagonal. In contrast to bulk systems, off-diagonal elements could be non-zero in systems with reduced symmetry, for example at surfaces.

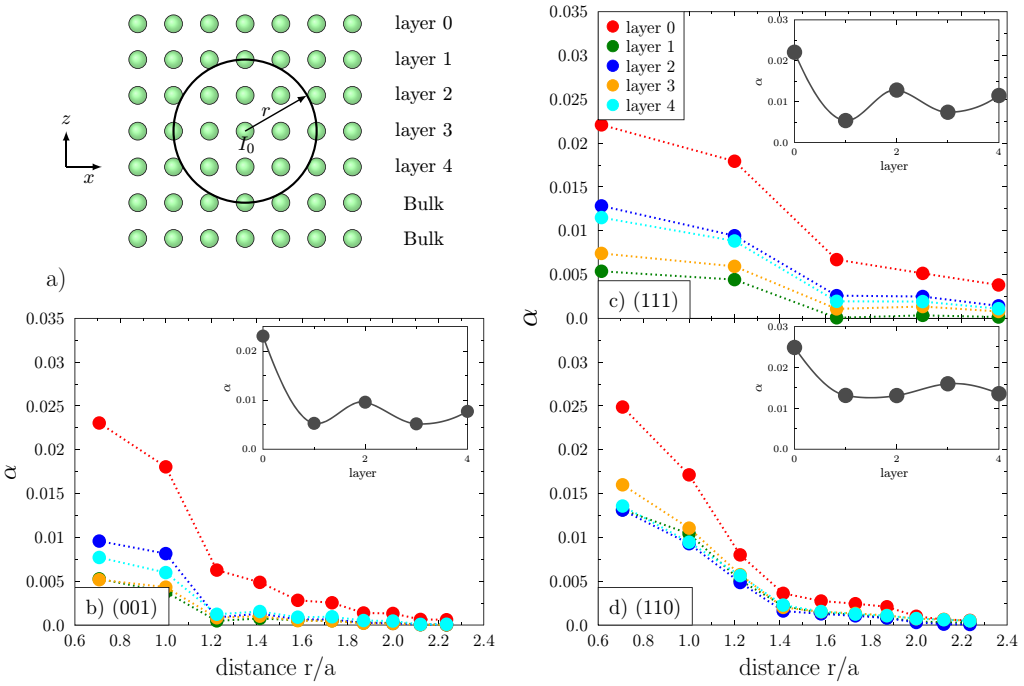

Figure 4. (a) Schematic view of the summation method in a cubic lattice to obtain $\alpha(r)$. For a given r all atoms are accounted for that are located on the circle. (b)–(d) Layer-resolved non-local damping constant for different Co surfaces: (b) (001), (c) (110) and (d) (111). The electron–phonon coupling Λ is 0.01 eV. The non-local character of the damping within the layers disappears within few nanometer distance; in contrast, a non-monotonic decrease of the damping constant with respect to the layer index is observed (layers are distinguished by colors). The damping does not depend significantly on the surface orientation.

3.2. Damping tensor at surfaces

In the following, we address the electronic contribution to the damping tensor $\boldsymbol{\alpha}$ at surfaces. As examples, we focus on (001), (110) and (111) surfaces of fcc-Co with Cu lattice constant 3.54 Å, addressing thick Co films on Cu surfaces.

The Rayleigh dissipation functional predicts energy transfer between neighboring sites $I \neq J$ [52, 53]. Hence, the energy transfer rate has to be considered as a non-local, rather than as a local (on-site) quantity [3]. In contrast, on-site contributions account for a local coupling to the lattice reservoir (phonons). To simplify the discussion, we define a shell-averaged damping tensor $\boldsymbol{\alpha}(r)$ by considering a reference site i_0 in layer n_0 ($I_0 = (n_0, i_0)$) and summing up contributions from all sites j in layer m ($m \neq n_0$ and $j \neq i_0$) that are located on a sphere with radius r (figure 4).

For all three surfaces, the energy transfer is short-ranged, as is evident from the decrease of α with distance r (figure 4). The damping depends also on the surface orientation: the nearest-neighbor α's differ slightly ($\alpha^{(001)}_{NN,I_0} = 0.023$, $\alpha^{(110)}_{NN,I_0} = 0.025$ and $\alpha^{(111)}_{NN,I_0)} = 0.022$), as can be explained qualitatively by the coordination numbers of site I_0 (8, 7 and 9 for (001), (110) and (111), respectively). If only nearest-neighbor hopping would be considered, a reduced coordination yields a small electron hopping probability (small band width), resulting in both a minute energy transfer and damping constant.

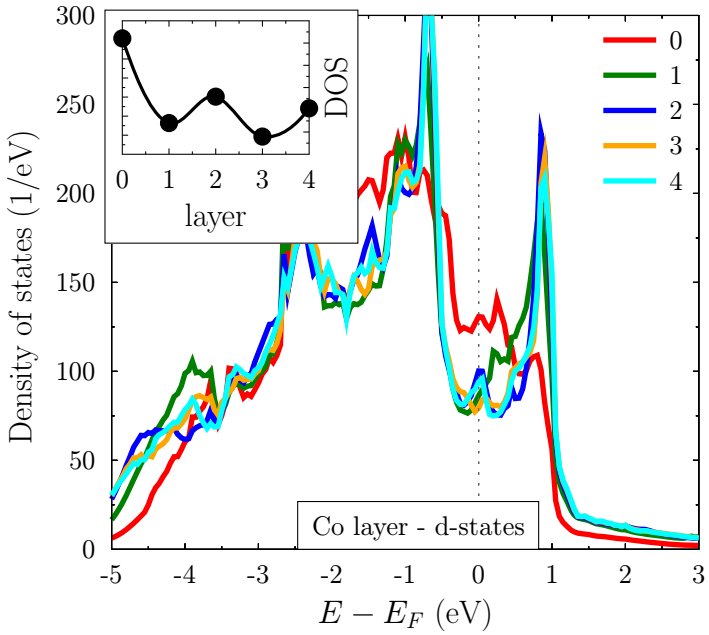

Figure 5. Layer-resolved DOS of d states in fcc Co(001). Layers are marked by different colors; the topmost layer is 0. The Fermi level is depicted as a dotted line. The inset shows the DOS at the Fermi level versus layer index (top surface layer $n = 0$).

α decreases with layer index (inset in figure 4). The topmost layer shows the largest dissipation for all three surfaces, which is in accordance with the fluctuation-dissipation theorem. NB: in the LLG equation, the fluctuation amplitude (that is the width of the Gaussian distribution of the random magnetic field [2]) reads $\alpha \cdot {}^{k_B T}/_{\gamma m}$; hence, the response at a temperature T is stronger at the surface than in the bulk. The dependence of α on the layer index is non-monotonous and exhibits oscillations; this finding is at variance with results reported in [54] but agrees with those in [23, 24]. The oscillations can be explained by the density of states of the d states which 'carry' the magnetic moment of Co.

The density of states of d orbitals at the Fermi level is largest for the surface layer (figure 5). It oscillates similarly to α; this coincidence has been already noticed in [7, 55]. The oscillations are explained by the behavior of t_{2g} and e_g states: the density of states (DOS) $n_{t_{2g}}(\varepsilon_F)$ decreases monotonically with layer index but $n_{e_g}(\varepsilon_F)$ shows an oscillatory behavior.

Eventually, we address how the non-locality of the Gilbert damping α_{ij} affects the magnetization dynamics in different layers, using (5) on a fs-time scale. The non-locality is relevant in an incoherent magnetic configuration, e.g. in demagnetization processes [55] or in nutation [56], both relevant on femtosecond or picosecond time scales; in case of a coherent precession of the magnetic moments, the sum in (5) can be replaced by an effective constant $\alpha_i^{\text{eff}} = \sum_j \alpha_{ij}$ [10]. We discuss its effect for the nutation in a two-layer thick Co film on Cu(111) [56]. Here, we include $\alpha(r)$ from Co(111) up to third-nearest neighbors ($r = 4.4$ Å) (figure 6). Here, the electron and spin temperature are zero; the electron–phonon coupling enters with $\Lambda = 0.01$ eV.

Assuming a linear temperature dependence of the electron–phonon coupling $\Lambda = BT_{\text{ph}}$ (e. g. $B = 0.011\,\text{eV}\,\text{K}^{-1}$ for nickel)—as in the Drude model [57]—a finite Λ requires a finite

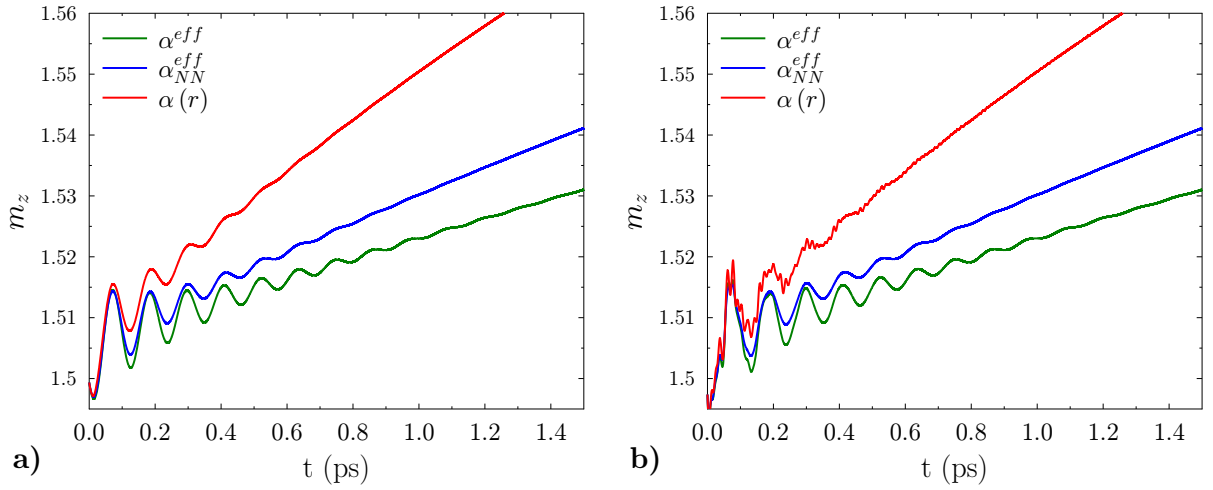

Figure 6. Nutation of a surface magnetic moment in a two layer thick Co film on Cu(111) of (a) a coherent and (b) a non-coherent spin state. m_z is shown versus time for different damping scenarios: considering the non-local α_{ij} (red); effective α integrated over the distance r (green, 0.083 for the surface and 0.021 for the subsurface layer), and effective α integrated over r and weighted by the coordination number (blue, 0.12 for the surface and 0.028 for the subsurface layer).

phonon temperature T_{ph}. Here, we choose a value of 1 K. In accordance with Ebert *et al* [7], this implies that the Kamberský model fails for zero phonon temperature because it results in an infinite Gilbert damping. Nevertheless, the chosen small T_{ph} allows the LLG equation to be applied for zero electron and spin temperatures.

An initial incoherent state is prepared by perturbing randomly the coherent precession around the anisotropy field at time $t = 0$. Then, an external magnetic field with a strength of $B = 5\,\mathrm{T}$ is abruptly switched on. We study three cases: accounting for (i) the non-local α_{ij}; (ii) an effective α by summing over the distances r; and (iii) an effective α by summing over distance r but weighted with the respective coordination numbers.

Both the nutation lifetime and the amplitude are reduced with higher damping, which supports the proportionality of the moment of inertia and the damping [58]. Case (ii) exhibits the smallest damping and, thus, a larger duration of the nutation. For case (i) the energy transfer to the neighboring sites accelerates the relaxation process compared to the other two cases. In contrast to the extended LLG equation used in [56], the present LLG equation (5) does not contain the magnetic moment of inertia and, thus, does not comprise a nutation term. Bhattacharjee *et al* [59] showed the existence of nutation without extension of the LLG equation. This finding is fully confirmed in our study by the increased nutation lifetime on a ps-time scale which differs from that in [56].

A coherent precession of all magnetic moments (figure 6(a)) gives a small phase shift (up to 10 fs), which is due to the direct coupling to the inert motion of site j. In an incoherent state, the evolution of j appears as a superimposed 'noisy signal' (red in figure 6(b)). According to the angular-momentum transfer present in the Heisenberg model, the energy transfer depends to the coordination: the higher the coordination number, the faster the relaxation. We conclude that anisotropic dissipation is advantageous in relaxation and switching processes in magnetic nanostructures.

4. Conclusion

We present a calculational method to obtain the Gilbert damping tensor based on the breathing Fermi-surface model. Within a TB approach the layer-dependence of the damping has been obtained. The non-local dissipation rate depends mildly on the surface orientation but strongly on the layer and on the distance to neighboring sites. In the tensor representation, the correlation to the reference magnetization results in a non-homogeneous dissipation, which suggests to consider the dependence of the Gilbert damping on the direction of the magnetic moments in future magnetization dynamics simulations.

We also studied the dependence of the Gilbert damping constant on the electron and spin temperatures. The damping increases with temperature, in contrast to experimental observations; this finding supports the fact that the phonon temperature is the major thermal contribution. The present comparably simple approximation of the electron–phonon coupling has to be improved in a future implementation. Nevertheless, the spin as well as the electron temperature should be considered in incoherent magnetization effects.

Acknowledgments

This work is supported by the *Sonderforschungsbereich* 762 'Functionality of Oxide Interfaces'. DT is a member of the International Max Planck Research School on Science and Technology of Nanostructures, Halle, Germany.

References

[1] Liu C, Mewes C, Chshiev M, Mewes T and Butler W H 2009 Origin of low Gilbert damping in half metals *Appl. Phys. Lett.* **95** 022509
[2] Skubic B, Hellsvik J, Nordsträom L and Eriksson O 2008 A method for atomistic spin dynamics simulations: implementation and examples *J. Phys.: Condens. Matter* **20** 315203
[3] Gilbert T L 2004 A phenomenological theory of damping in ferromagnetic materials *IEEE Trans. Magn.* **40** 6
[4] Fuchs G D *et al* 2007 Spin-torque ferromagnetic resonance measurements of damping in nanomagnets *Appl. Phys. Lett.* **91** 062507
[5] Oogane M, Wakitani T, Yakata S, Yilgin R, Ando Y, Sakuma A and Miyazaki T 2006 Magnetic damping in ferromagnetic thin films *Japan. J. Appl. Phys.* **45** 3889–91
[6] Etz C, Costa M, Eriksson O and Bergman A 2012 Accelerating the switching of magnetic nanoclusters by anisotropy-driven magnetization dynamics *Phys. Rev.* B **86** 224401
[7] Ebert H, Mankovsky S, Ködderitzsch D and Kelly J P 2011 *Ab initio* calculation of the Gilbert damping parameter via linear response formalism *Phys. Rev. Lett.* **107** 066603
[8] Kuneš J and Kamberský V 2002 First-principles investigation of the damping of fast magnetization precession in ferromagnetic 3d metals *Phys. Rev.* B **65** 212411
[9] Kamberský V 1984 *Czech. J. Phys.* B **34** 1111
[10] Mankovsky S, Ködderitzsch D, Woltersdorf G and Ebert H 2013 First-principles calculation of the Gilbert damping parameter via the linear response formalism with application to magnetic transition-metals and alloys arXiv:1301.2114v1 [cond-mat.other]
[11] Gilmore K, Idzerda Y U and Stiles M D 2007 Identification of the dominant precession-damping mechanism in Fe, Co and Ni by first-principles calculations *Phys. Rev. Lett.* **99** 027204
[12] Fähnle M and Steiauf D 2006 Breathing Fermi surface model for noncollinear magnetization: a generalization of the Gilbert equation *Phys. Rev.* B **73** 184427

[13] Steiauf D and Fähnle M 2005 Damping of spin dynamics in nanostructures: an *ab initio* study *Phys. Rev.* B **72** 064450
[14] Bhagat S M and Lubitz P 1974 Temperature variation of ferromagnetic relaxation in the 3d transition metals *Phys. Rev.* B **10** 179–85
[15] Heinrich B and Frait Z 1966 Temperature dependence of the FMR linewidth of iron single crystal platelets *Phys. Status Solidi* **16** K11–4
[16] Schreiber F, Pflaum J, Frait Z, Miihge Th and Pelzl J 1995 Gilbert damping and g-factor in Fe_xCo_{1-x} alloy films *Solid State Commun.* **93** 965–8
[17] Inaba N, Asanuma H, Igarashi S, Mori S, Kirino F, Koike K and Morita H 2006 Damping constants of Ni–Fe and Ni–Co alloy thin films *IEEE Trans. Magn.* **42** 10
[18] Trunova A 2009 Ferromagnetische resonanz an oxidfreien magnetischen Fe und FeRh nanopartikeln *PhD Thesis* Universität Duisburg-Essen
[19] Song H-S, Lee K-D, Sohn J-W, Yang S-H, Parkin S S P, You C-Y and Shin S-C 2013 Observation of the intrinsic Gilbert damping constant in Co/Ni multilayers independent of the stack number with perpendicular anisotropy *Appl. Phys. Lett.* **102** 102401
[20] Mizukami S, Sajitha E P, Watanabe D, Wu F, Miyazaki T, Naganuma H, Oogane M and Ando Y 2010 Gilbert damping in perpendicularly magnetized Pt/Co/Pt films investigated by all-optical pump–probe technique *Appl. Phys. Lett.* **96** 152502
[21] Lenz K, Wende H, Kuch W, Baberschke K, Nagy K and Jánossy A 2006 Two-magnon scattering and viscous Gilbert damping in ultrathin ferromagnets *Phys. Rev.* B **73** 144424
[22] Walowski J 2007 Non-local/local Gilbert damping in nickel and permalloy thin films *Master's Thesis* IV. Pysikalisches Institut (Institut für Halbleiterphysik) der Georg-August-Universität zu Göttingen
[23] Umetsu N, Miura D and Sakuma A 2012 Theoretical study on Gilbert damping of nonuniform magnetization precession in ferromagnetic metals *J. Phys. Soc. Japan* **81** 114716
[24] Brataas A, Tserkovnyak Y and Bauer G 2011 Magnetization dissipation in ferromagnets from scattering theory *Phys. Rev.* B **84** 054416
[25] Vittoria C, Yoon S D and Widom A 2010 Relaxation mechanism for ordered magnetic materials *Phys. Rev.* B **81** 014412
[26] Grotendorst J, Attig N, Blügel S and Marx D 2009 *Multiscale Simulation Methods in Molecular Sciences* (Julich: Julich Supercomputing Centre) pp 1–592
[27] Slater J C and Koster G F 1954 Simplified LCAO method for the periodic potential problem *Phys. Rev.* **94** 1498–524
[28] Harrison W A 1980 *Electronic Structure and the Properties of Solids* (San Francisco, CA: Freeman)
[29] Goldberg D E 1989 *Genetic Algorithms in Search, Optimization and Machine Learning* (Reading, MA: Addison-Wesley)
[30] Starrost F, Bornholdt S, Solterbeck C and Schattke W 1996 Band-structure parameters by genetic algorithm *Phys. Rev.* B **53** 12 549
[31] Zhong W, Overney G and Tománek D 1993 Structural properties of Fe crystal *Phys. Rev.* B **47** 1
[32] Liu G, Nguyen-Manh D, Liu B G and Pettifor D G 2005 Magnetic properities of point defects in iron within the tight-binding-bond Stoner model *Phys. Rev.* B **71** 174115
[33] Okutani M and Jo T 2000 Orbital magnetic moment in superlattices of transition metals *J. Phys. Soc. Japan* **69** 598–606
[34] Zabloudil J, Hammerling R, Szunyogh L and Weinberger P (ed) 2005 *Electron Scattering in Solid Matter* (Berlin: Springer)
[35] Henk J and Schattke W 1993 A subroutine package for computing Green's functions of relaxed surfaces by the renormalization method *Comput. Phys. Commun.* **77** 69
[36] Bödicker A, Schattke W, Henk J and Feder R 1994 Interface electronic structure by the renormalization method: theory and application to Sb/GaAs *J. Phys.: Condens. Matter.* **6** 1927
[37] Agranat M B, Ashitkov S I, Granovskĭi A B and Rukman G I 1984 Interaction of picosecond laser pulse with the electron, spin, phonon subsystems of nickel *Zh. Eksp. Teor. Fiz.* **86** 1376–9

[38] Kirilyuk A, Kimel A V and Rasing T 2010 Ultrafast optical manipulation of magnetic order *Rev. Mod. Phys.* **82** 2731
[39] Laufer P M and Papaconstantopoulos D A 1987 Tight-binding coherent-potential approximation study of the electronic states of palladium-noble-metal alloys *Phys. Rev.* B **35** 17
[40] Blackman J A and Esterling D M 1971 Generalized locator-coherent-potential approach to binary alloys *Phys. Rev.* B **4** 8
[41] Landau L D and Lifshitz L M 1935 On the theory of the dispersion of magnetic permeability in ferromagnetic bodies *Phys. Z. Sowjetunion* **8** 153–69
[42] Liechtenstein A I, Katsnelson M I, Antropov V P and Gubanov V A 1987 Local spin density functional approach to the theory of exchange interactions in ferromagnetic metals and alloys *J. Magn. Magn. Mater.* **67** 65
[43] Böttcher D 2010 Theoretische Beschreibung der Magnetisierungsdynamik von Nanostrukturen *Master's Thesis* Institut für Physik, Martin Luther University Halle-Wittenberg, Halle (Saale), Germany
[44] Kirilyuk A, Kimel A V and Rasing T 2013 Laser-induced magnetization dynamics and reversal in ferrimagnetic alloy *Rep. Prog. Phys.* **76** 026501
[45] Staunton J, Gyorffy B L, Pindor A J, Stocks G M and Winter H 1984 The 'disordered local moment' picture of itinerant magnetism at finite temperatures *J. Magn. Magn. Mater.* **45** 15–22
[46] Gyorffy B L, Pindor A J, Staunton J, Stocks G M and Winter H 1985 A first-principles theory of ferromagnetic phase transitions in metals *J. Phys. F: Met. Phys.* **15** 1337–86
[47] Faulkner J S 1977 Scattering theory and cluster calculations *J. Phys. C: Solid State Phys.* **10** 4661
[48] Böttcher D, Ernst A and Henk J 2012 Temperature-dependent Heisenberg exchange coupling constants from linking electronic-structure calculations and Monte Carlo simulations *J. Magn. Magn. Mater.* **324** 610
[49] Binder K (ed) 1979 *Monte Carlo Methods in Statistical Physics* (Berlin: Springer)
[50] Papaconstantopoulos D A and Mehl M J 2003 The Slater–Koster tight-binding method: a computationally efficient and accurate approach *J. Phys.: Condens. Matter.* **15** R413
[51] Kamberský V 2007 Spin–orbital Gilbert damping in common magnetic metals *Phys. Rev.* B **76** 134416
[52] Torby B 1984 Energy methods *Advanced Dynamics for Engineers* (*HRW Series in Mechanical Engineering*) (New York: Holt, Rinehart and Winston) 1–426
[53] Meirovitch L (ed) 1970 *Methods of Analytical Dynamics* (New York: McGraw-Hill)
[54] Barati E, Cinal M, Edwards D M and Umerski A 2013 Calculation of Gilbert damping in ferromagnetic films *EPJ Web Conf.* **40** 18003
[55] Mann A *et al* 2012 Insights into ultrafast demagnetization in pseudogap half-metals *Phys. Rev. X* **2** 041008
[56] Böttcher D and Henk J 2012 Significance of nutation in magnetization dynamics of nanostructures *Phys. Rev.* B **86** 020404
[57] Lin Z and Zhigilei L V 2007 Temperature dependences of the electron–phonon coupling, electron heat capacity and thermal conductivity in Ni under femtosecond laser irradiation *Appl. Surf. Sci.* **253** 6295–300
[58] Ciornei M-C, Rubi J M and Wegrowe J-E 2011 Magnetization dynamics in the inertial regime: nutation predicted at short time scales *Phys. Rev.* B **83** 020410
[59] Bhattacharjee S, Bergman A, Taroni A, Hellsvik J, Sanyal B and Eriksson O 2012 Theoretical analysis of inertia-like switching in magnets: applications to a synthetic antiferromagnet *Phys. Rev. X* **2** 011013